THE UNIVERSITY *of* EDINBURGH

Edinburgh Research Explorer

Developmental and Degenerative Cardiac Defects in the Taiwanese Mouse Model of Severe Spinal Muscular Atrophy

Citation for published version:
Maxwell , GK, Szunyogova, E, Shorrock, H, Gillingwater, T & Parson, SH 2018, 'Developmental and Degenerative Cardiac Defects in the Taiwanese Mouse Model of Severe Spinal Muscular Atrophy', *Journal of Anatomy*. https://doi.org/10.1111/joa.12793

Digital Object Identifier (DOI):
10.1111/joa.12793

Link:
Link to publication record in Edinburgh Research Explorer

Document Version:
Peer reviewed version

Published In:
Journal of Anatomy

OPEN ACCESS

1   **Developmental and Degenerative Cardiac Defects in the Taiwanese Mouse Model of**
2   **Severe Spinal Muscular Atrophy**
3

4   *Gillian K. Maxwell[1], Eva Szunyogova[1,3], Hannah K. Shorrock[2,3], Thomas H. Gillingwater[2,3] and*
5   *Simon H. Parson[1,3]*
6
7
8
9
10   [1]Institute for Medical Science, University of Aberdeen, Aberdeen, Scotland, AB25 2ZD
11   [2]Edinburgh Medical School: Biomedical Sciences, University of Edinburgh, Edinburgh,
12   Scotland, EH8 9AG
13   [3]Euan MacDonald Centre for Motor Neurone Disease Research, University of Edinburgh,
14   Edinburgh, Scotland, EH16 4SB
15
16
17   Running title: Heart Defects in SMA
18
19   Key words: Cardiovascular, cardiac, stress, cell death, ventricle, septum

Abstract

20

21

22 Spinal muscular atrophy (SMA), an autosomal recessive disease caused by a decrease in
23 levels of the Survival Motor Neuron (SMN) protein, is the most common genetic cause of
24 infant mortality. Although neuromuscular pathology is the most severe feature of SMA,
25 other organs and tissues, including the heart, are also known to be affected in both patients
26 and animal models. Here, we provide new insights into changes occurring in the heart,
27 predominantly at pre- and early-symptomatic ages, in the Taiwanese mouse model of
28 severe SMA. Thinning of the interventricular septum and dilation of the ventricles occurred
29 at pre- and early-symptomatic ages. However, the left ventricular wall was significantly
30 thinner in SMA mice from birth, occurring prior to any overt neuromuscular symptoms.
31 Alterations in collagen IV protein from birth indicated changes to the basement membrane
32 and contributed to the abnormal arrangement of cardiomyocytes in SMA hearts. This raises
33 the possibility that developmental defects, occurring prenatally, may contribute to cardiac
34 pathology in SMA. In addition, cardiomyocytes in SMA hearts exhibited oxidative stress at
35 pre-symptomatic ages and increased apoptosis during early-symptomatic stages of disease.
36 Heart microvasculature was similarly decreased at an early-symptomatic age, likely
37 contributing to the oxidative stress and apoptosis phenotypes observed. Finally, an
38 increased incidence of blood retention in SMA hearts post-fixation suggests the likelihood of
39 functional defects, resulting in blood pooling. These pathologies mirror dilated
40 cardiomyopathy, with clear consequences for heart function that would likely contribute to
41 potential heart failure. Our findings add significant additional experimental evidence in
42 support of the requirement to develop systemic therapies for SMA capable of treating non-
43 neuromuscular pathologies.

44

Introduction

46

47 Our understanding of the pathogenesis of spinal muscular atrophy (SMA) remains
48 incomplete, despite its classification as a single gene disorder and a major genetic cause of
49 infant mortality. The ubiquitously expressed Survival Motor Neurone protein (SMN) –
50 named due to the predominant motor neurone loss seen in SMA (Werdnig, 1891; Hoffmann,
51 1892) – is produced from two genes in humans, with the majority of full-length protein
52 produced by the *SMN1* gene (Lorson *et al.,* 1999). In SMA, an autosomal recessive disease,
53 mutations in the *SMN1* gene leave the *SMN2* gene alone to produce small amounts of full-
54 length, functional SMN protein (Lefebvre *et al.,* 1995). This is sufficient to prevent
55 embryonic lethality but results in the pathology of SMA.

56

57 SMA is primarily characterised by loss of α-motor neurones in the spinal cord, causing
58 denervation and resulting atrophy of skeletal muscle (Lunn and Wang, 2008; Powis *et al.,*
59 2016a). However, a range of non-neuromuscular pathologies are also now apparent
60 (reviewed in: Hamilton and Gillingwater, 2013; Shababi *et al.,* 2014; Nash *et al.,* 2016),
61 including abnormalities affecting the liver (Vitte *et al.,* 2004; Szunyogova *et al.,* 2016), lung
62 (Schreml *et al.,* 2012), pancreas (Bowerman *et al.,* 2012; Bowerman *et al.,* 2014), spleen
63 (Thomson *et al.,* 2016; Deguise *et al.,* 2017; Khairallah *et al.,* 2017), testis (Ottesen *et al.,*
64 2016), intestines (Sintusek et al., 2016) and the vascular system (Shababi *et al.,* 2012;

65   Somers *et al.,* 2012; Sintusek *et al.,* 2016; Somers *et al.,* 2016). Amongst these, cardiac
66   abnormalities were first putatively described in SMA patients ~60 years ago (Sterne and
67   Lavieuville, 1964; Gardner-Medwin *et al.,* 1967), but are only now becoming accepted as a
68   potentially core aspect of SMA, particularly in severe forms of the disease (Wijngaarde *et*
69   *al.,* 2017).
70
71   In patients, cardiac defects have been described across mild and severe forms of SMA,
72   commonly falling into two major categories: structural defects and arrhythmias. Congenital
73   heart defects, including atrial septal defects, ventricular septal defects and hypoplastic
74   aortic arch, are the most common structural defects observed in SMA patients (Møller *et al.,*
75   1990; Burglen *et al.,* 1995; Mulleners *et al.,* 1996; Jong *et al.,* 1998; El-Matary *et al.,* 2004;
76   Cook *et al.,* 2006; Sarnat and Trevenen *et al.,* 2007; Vaidla *et al.,* 2007; Menke *et al.,* 2008;
77   Araujo *et al.,* 2009; Grotto *et al.,* 2016; Krupickova *et al.,* 2017). However, pulmonary
78   hypertension, ventricular enlargement, systolic murmurs and cardiomyopathies have also
79   been reported (Tanaka *et al.,* 1976; Tanaka *et al.,* 1977; Kimura *et al.,* 1980; Møller *et al.,*
80   1990; Distefano *et al.,* 1994; Elkohen *et al.,* 1996; Finsterer *et al.,* 1999; El-Matary *et al.,*
81   2004; Collado-Ortiz *et al.,* 2007; Vaidla *et al.,* 2007; Menke *et al.,* 2008; Kuru *et al.,* 2009). In
82   the case of arrhythmias, bradycardias are most predominant in children with SMA, although
83   heart block and ECG tremors have also been noted (Tanaka *et al.,* 1976; Kimura *et al.,* 1980;
84   Dawood and Moosa, 1983; Coletta *et al.,* 1989; Finsterer *et al.,* 1999; Arai *et al.,* 2005;
85   Hachiya *et al.,* 2005; Takahashi *et al.,* 2006; Rudnik-Schöneborn *et al.,* 2008; Roos *et al.,*
86   2009; Haliloglu *et al.,* 2015; Grotto *et al.,* 2016). Together these findings do not immediately
87   suggest a common or consistent aetiology. Therefore, further work is required to
88   understand the degree to which these represent primary or secondary causative co-
89   morbidities.
90
91   Heart defects have been reliably reproduced in both severe and mild mouse models of SMA.
92   These include; structural changes represented by thinning of the interventricular septum
93   (IVS) and left ventricular (LV) wall (Bogdanik *et al.,* 2015; Schreml *et al.,* 2013; Shababi *et al.,*
94   2010); dilated cardiomyopathy (Bevan *et al.,* 2010; Heier *et al.,* 2010; Schreml *et al.,* 2013;
95   Bogdanik *et al.,* 2015); and increased fibrosis and oxidative stress (Shababi *et al.,* 2010). In
96   both severe and mild mouse models, reports of both a decreased ejection fraction (Bevan *et*
97   *al.,* 2010; Bogdanik *et al.,* 2015) and arrhythmias, particularly bradycardia (Bevan *et al.,*
98   2010; Heier *et al.,* 2010; Shababi *et al.,* 2010; Biondi *et al.,* 2012; Bogdanik *et al.,* 2015),
99   indicate functional changes. Significantly, in the very mild 'Burgheron' mouse model, some
100   mice die from severe cardiomyopathy rather than the effects of neuromuscular pathology
101   (Bogdanik *et al.,* 2015). However, our understanding of these heart defects is still
102   incomplete.
103
104   Heart defects in SMA represent only one aspect of disruption to the cardiovascular system.
105   Other notable changes include a pronounced decrease in blood vessel density in skeletal
106   muscle of both patients and a severe mouse model (Somers *et al.,* 2012; Somers *et al.,*
107   2016), and in the spinal cord (Somers *et al.,* 2016), intestines (Sintusek *et al.,* 2016) and
108   heart (Shababi *et al.,* 2012) of severe SMA mouse models. Distal necrosis is seen in the
109   fingers and toes of patients (Araujo *et al.,* 2009; Rudnik-Schöneborn *et al.,* 2010), and in the
110   ears and tail of mouse models (Hsieh-Li *et al.,* 2000; Tsai *et al.,* 2006; Narver *et al.,* 2008;
111   Hua *et al.,* 2010; Riessland *et al.,* 2010; Schreml *et al.,* 2013; Bogdanik *et al.,* 2015; Catapano

112 *et al.,* 2016). This necrosis in patients is resolved by anticoagulant treatment, suggesting
113 that these are thrombotic occlusions (Araujo *et al.,* 2009). Finally, there is consistent
114 evidence of persistent extramedullary haematopoiesis in SMA. In a severe mouse model,
115 the liver is undergoing erythropoiesis; it has an increased number of megakaryocytes;
116 elevated platelet levels; and higher levels of normoblasts (nucleated red blood cells) in
117 blood samples (Szunyogova *et al.,* 2016). Similarly, the spleen of a severe SMA mouse also
118 has increased megakaryocyte density and immature architecture indicative of ongoing
119 haematopoiesis (Thomson *et al.,* 2016). Abnormalities of the spleen have also been
120 reported in SMA patients, with red pulp congestion and the presence of erythroid
121 precursors (Thomson *et al.,* 2016).
122
123 Given the growing awareness of cardiovascular defects in SMA, we set out to undertake a
124 detailed morphological assessment of the heart in the 'Taiwanese' mouse model of severe
125 SMA. By focussing on the period between birth and the first appearance of overt
126 neuromuscular symptoms, we attempted to identify the initiation of cardiovascular defects,
127 giving a better understanding of mechanisms underlying these phenotypes in SMA.
128
129 We report significant structural and molecular defects in the heart, prior to, or in tandem
130 with overt neuromuscular pathology; key molecular targets of SMN-depletion in the heart;
131 and suggest a multifactorial cardiovascular system pathology.
132

Methods

134
135 **Mice**
136
137 The Taiwanese SMA mouse model on a congenic FVB background was used to replicate a
138 severe phenotype of SMA. Taiwanese SMA mice were maintained as breeding pairs under
139 standard specific-pathogen-free conditions in animal care facilities at Edinburgh University
140 (Hsieh-Li *et al.,* 2000; Riessland *et al.,* 2010; Powis *et al.,* 2016b). Offspring littermates were
141 either heterozygous for Smn knockout (*Smn*$^{+/-}$;*SMN2*$^{tg/0}$) and used as controls, or
142 homozygous (*Smn*$^{-/-}$;*SMN2*$^{tg/0}$) and used as SMA disease model. All experimental protocols
143 were approved by Edinburgh University internal research and ethics committees and were
144 carried out in accordance with licenses obtained from the United Kingdom Home Office
145 under the Animals (Scientific Procedures) Act 1986. Genotyping of mice was carried out *via*
146 standard PCR protocols (Wishart *et al.,* 2014). Day of birth is defined as postnatal day 1 (P1).
147
148 **Tissue Processing**
149
150 Hearts were harvested between P1-P8 from mice sacrificed by intraperitoneal injection of
151 sodium pentobarbital in accordance with UK guidance and rules for the use of animals in
152 research. Hearts were then fixed for 4hrs in 4 % paraformaldehyde (PFA) before undergoing
153 cryoprotection in 30 % sucrose and embedding in OCT. Hearts were cryo-sectioned at a
154 thickness of 7 μm. Sections then underwent either basic haematoxylin and eosin (H&E)
155 staining or immunohistochemistry.
156
157 **Immunohistochemisty**

158
159   Heart sections were incubated overnight at 4 °C with the following primary antibodies:
160   rabbit polyclonal anti-Collagen IV (Millipore, AB756P), rabbit polyclonal anti-Ki67 (Abcam,
161   ab16667) and rat monoclonal anti-Ly76 (Abcam, ab91113); and for 2 hours with the
162   corresponding secondary antibodies: Cy3 Goat anti-rabbit IgG (H+L) (Life Technologies, A-
163   10520) and Cy3 goat anti-rat IgG (H+L) (Life Technologies, A-10522). 3x10 minute washes in
164   PBT (0.1M PBS with 0.1 % Tween-20) and 0.1 M PBS were carried out between and after
165   antibody incubation. Rhodamine labelled Griffonia Lectin 1 (GSL-1) was used to stain
166   vasculature. Sections were coverslipped using mowiol mounting media (10% Mowiol
167   (Sigma-Aldrich, 81381), 20 % Glycerol, 50 % 0.2 M Tris buffer pH 8.5, 3 % 1,4-
168   diazobicyclooctane made up in distilled water) containing DAPI. Sections were imaged using
169   Nikon eclipse e400 microscope (10x objective) and its images captured using QICAM Fast
170   1394 camera and Improvision Velocity 4 image capture software.
171
172   **Quantitative Western Blotting**
173
174   Quantitative Western blotting was carried out on 3 hearts per genotype (Eaton *et al.,* 2014).
175   Briefly, hearts were digested in RIPA buffer containing 2.5 % Halt protease inhibitor cocktail
176   and homogenised. BCA assay was carried out to quantify protein concentration of individual
177   samples. 15 µg of protein was loaded per well. Samples were separated by electrophoresis
178   on precast Bolt^{TM} 4-12 % Bis-Tris Plus Gels (NW04120BOX) and then transferred to
179   nitrocellulose membranes using semi-dry I-Blot$^®$ transfer system (Invitrogen, UK). Reversible
180   total protein stain was carried out using Li-COR Revert total protein stain and wash solution
181   (LI-COR, 926-11011). To revert the membrane 0.1 % sodium hydroxide in 30 % methanol in
182   water was used. Membranes were incubated overnight at 4 ^{o}C with the following primary
183   antibodies: rabbit polyclonal anti-caspase-3 (Abcam, ab13847), rabbit polyclonal anti-
184   angiotensin II receptor 1 (AT-1) (Abcam, ab18801) and goat polyclonal anti-platelet
185   endothelial cell adhesion molecule-1 (PECAM-1) (R&D Systems, AF3628); diluted in SeaBlock
186   blocking buffer (ThermoFisher Scientific, 37527) with Tween-20. Corresponding secondary
187   antibodies, donkey anti-rabbit Alexa Fluor$^®$ 680 IgG (H+L) (Abcam, ab186692) and donkey
188   anti-goat Alexa Fluor$^®$ 790 IgG (H+L) (Abcam, ab175784), were incubated at room
189   temperature for 2 hours. 6x10 minute washes with 0.1 M PBS were carried out between and
190   after antibody incubation. Membranes were imaged using Li-COR Odyssey Scanner and
191   Software. Due to alterations in the expression levels of many standard loading control
192   proteins in SMA tissues, total protein was used to normalise protein expression (Eaton et al.,
193   2013). Image Studio Lite was used for quantification of Western blots.
194
195   **Heart Quantification**
196
197   In all analyses, folded or damaged heart sections were rejected. ImageJ was used to
198   measure the area of the heart and ventricles, for cell counts, and for red blood cell density
199   analysis. A protractor generated in Adobe Photoshop was used to quantify IVS and LV walls.
200
201   *Quantification of Structural Changes to the Heart*: IVS width, LV wall width and ventricular
202   lumen area were measured from 4 H&E stained slides, containing ~8 heart sections per
203   heart (~30 in total per heart), from the same relative area, i.e. between the apex and the
204   atrioventricular septum. Images were captured at 40x magnification and under the same

205 exposure. The freehand selection tool in Image J was used to measure the area of the heart
206 and the left and right ventricles in calibrated images. In Adobe Photoshop, to measure the
207 IVS and the LV wall, the largest rectangle of best fit was placed in the LV and the centre was
208 found. From here, lines of 20° were drawn radially to intersect the IVS or LV wall and the
209 ruler tool was used to measure between points on these lines. Distance was either
210 measured between the edge of the two ventricles for IVS width or between the left
211 ventricle wall and the edge of the heart for LV wall width.
212
213 *Ly76 Density Quantification*: The density of Ly76 positive cells was measured from ~8
214 sections taken from the same relative area in each heart. Images were captured at 40x
215 magnification and under the same exposure. Brightness and contrast were enhanced in
216 Adobe Photoshop. The enhanced images were then converted into binary in ImageJ, where
217 Ly76 positive cells were assigned black, and the background white. A ratio of black to white
218 pixels for the whole heart area could then be calculated, allowing a relative value for Ly76
219 positive cell area relative to heart area, expressed as a percentage.
220
221 *Cell Density and Ki67 Positive Cell Quantification*: Cell density was calculated from ~8
222 sections at the same relative area in each heart. From each heart section 6 different images
223 at 400x magnification were captured fully composed of tissue at the same exposure, from
224 the same 6 areas for each heart, i.e. in the LV wall, the IVS and the RV wall. DAPI-blue
225 channels and Ki67-red channels were merged in Adobe Photoshop. ImageJ was then used to
226 count the number of DAPI positive nuclei only, and both DAPI and Ki67 positive nuclei
227 combined in the field of view. The number of Ki67 and DAPI positive cells combined was
228 expressed as a percentage of total number of DAPI positive cells.
229
230 *Statistics:* All experimental groups consisted of a minimum of 3 different animals, which has
231 previously shown to be sufficient to attain statistical significance (Szunyogova *et al.,* 2016).
232 All graphs are shown as mean ± SEM. Unpaired two-tailed t-test and two-way ANOVA were
233 carried out using PRISM, where * $< p0.05$; ** $< p0.01$; *** $< p0.001$.
234

235 Results
236
237 **Gross Heart Morphology is Altered in SMA Mice**
238
239 Initial assessment of hearts from SMA mice revealed no obvious gross anatomical
240 disorganisation across all ages studied from P1 and P3 (pre-symptomatic), through P5 (early
241 symptomatic) and P8 (symptomatic), but SMA hearts were smaller when compared to
242 control (Fig. 1A). When heart weight was expressed relative to body weight (which is lower
243 in late symptomatic SMA mice; see Powis *et al*., 2016b), there was no significant difference
244 between SMA and control hearts at any of the ages examined (P1,3,5,8: ns > 0.05: Fig. 1B).
245 Upon closer observation of transverse sections of the heart stained with H&E, SMA hearts
246 appeared to have thinner ventricular walls, and larger ventricles, which were congested
247 with blood (Fig. 1C). IVS and LV wall measurements have been made previously (Bevan *et*
248 *al.,* 2010; Shababi *et al.,* 2010), however, the time course of ventricle dilation has not been
249 analysed. Quantification revealed that the relative area of the heart comprised of the
250 ventricles was significantly greater in SMA, at pre (P3) and early (P5) -symptomatic ages

251 suggesting enlargement of the ventricles occurs early in the SMA phenotype (P1: ns > 0.05;
252 P3: *** <0.001; P5: * < 0.05) (Fig. 1D). Furthermore, the IVS and LV wall, which together
253 comprise the main muscle mass of the heart, were thinner, relative to body weight, in SMA
254 hearts from an early age (Fig. 1E and 1F). The IVS was significantly thinner at pre and early-
255 symptomatic ages (P1: ns > 0.05; P3: * < 0.05; P5: ** < 0.01), whereas the LV wall was
256 significantly thinner from birth onwards (P1: * < 0.05; P3: *** < 0.001; P5: * < 0.05).

258 These data not only show significant changes in the heart wall and IVS in the Taiwanese
259 SMA mouse model, but moreover indicate that they develop in pre-symptomatic animals,
260 with evidence of cardiac defects present at birth. This suggests that heart pathology is likely
261 to represent a primary event in SMA, and is not simply a secondary consequence of
262 neuromuscular pathology.

264 **Cardiomyocytes are Disorganised in the SMA Heart**

266 Given the gross pathology evident in the heart wall of SMA mice, we next investigated the
267 fine structure of the heart to determine the likely aetiology of the defects in the IVS and LV
268 wall. To determine the arrangement of cardiomyocytes, collagen IV immunohistochemistry
269 was used to highlight surrounding basement membranes from birth to early-symptomatic
270 ages (P1, P3 and P5). The basement membrane surrounds the cardiomyocytes providing
271 structural support and is important during heart development for the formation of
272 sarcomeres.

274 At P5 the LV wall in control hearts was clearly formed by 3 layers of cardiac muscle;
275 superficial oblique, cylindrical middle, and deep longitudinal layers (Fig. 2A v and 2B i). The
276 middle layer in particular was most pronounced, containing strands of cardiomyocytes
277 which spiralled out anti-clockwise from the LV, twisting in the orientation of heart
278 contraction (Greenbaum *et al.,* 1981; Sedmera and McQuinn, 2009). This structure not only
279 ensures a coherent electrical impulse transfer, but is essential for the twisting motion of the
280 ventricles observed during contraction of the heart. At birth, this spiral structure
281 surrounding the LV was beginning to develop in the control heart (Fig. 2A i). In contrast, the
282 heart wall in SMA was disorganised with no apparent development of cardiomyocyte
283 orientation between birth and P5 (Fig. 2A ii, 2A iv, 2A vi and 2B ii). The appearance was in
284 fact similar to an embryonic heart, where muscle is arranged circumferentially around the
285 ventricle rather than radiating from it (Sedmera and McQuinn, 2009).

287 During embryonic development trabeculations are formed in the ventricles prior to the
288 formation of the coronary vasculature to increase surface area for nutrient uptake (Sedmera
289 *et al.*, 2000). An essential stage in increasing the mass of the compact muscular wall of the
290 heart is compaction of these trabeculae, which coincides with the formation of the coronary
291 blood supply (Sedmera *et al.*, 2000). In the control heart, nearer the luminal wall of the LV,
292 trabeculations can often be seen. These trabeculations are sparse, do not penetrate far into
293 the lumen, and appear large enough to allow the growth of a blood supply to these cells

294 (Fig. 2B iii). In SMA, these trabeculations were greater in number, projected further into the
295 lumen, and were very thin, with little capacity for a blood supply to invade (Fig. 2B iv). This
296 occured from birth, where P1 SMA hearts had little definition between the compact wall
297 and the ventricles (Fig. 2A ii) and was still present at early-symptomatic (P5) ages (Fig. 2A vi).
298
299 Collagen IV immunostaining, used to visualise cardiomyocyte arrangement, showed a non-
300 uniform pattern of labelling with an apparent decrease in staining, particularly towards the
301 superficial surface in the SMA hearts compared to control hearts. This suggests a defect in
302 the basement membrane, of which collagen IV is a key component and which is essential to
303 maintain the organisation of cardiomyocytes in the heart. Further, a significant global
304 decrease in collagen IV expression in SMA hearts was demonstrated by quantitative
305 Western blotting at birth (P1: *<0.05) (Fig. 2C). Importantly, collagen IV interacts directly
306 with SMN protein (Fuller *et al.,* 2016), suggesting a potential mechanistic link between SMN
307 depletion and heart wall disorganisation.
308
309 **SMA Hearts Have a Decreased Number of Cardiomyocytes Associated with Increased**
310 **Apoptosis**
311
312 To establish the cellular basis of the changes in SMA heart structure, cardiomyocytes were
313 specifically investigated from birth (P1) through to early-symptomatic ages (P5). SMA hearts
314 showed a significant decrease in cardiomyocyte number per unit area (density) at pre- (P3)
315 and early- (P5) symptomatic ages but not at birth (P1: ns > 0.05; P3: **<0.01; P5: ***<
316 0.001) (Fig 3B). To establish the nature of this decrease in cardiomyocyte density, cell
317 proliferation and apoptosis were analysed. Heart sections were stained with Ki67 (Fig. 3A),
318 a proliferation marker expressed during all phases of division (Scholzen and Gerdes, 2000),
319 however, no significant difference in the number of proliferating cells between control and
320 SMA was observed between birth and P5 (P1: ns > 0.05; P3: ns > 0.05; P5: ns > 0.05) (Fig 3C).
321 Apoptosis was analysed by Western blot for caspase-3, involved in the activation cascade of
322 caspases responsible for apoptosis execution (Porter and Jänicke, 1999), which showed a
323 significant increase in early-symptomatic SMA hearts (P1: ns > 0.05; P3: ns > 0.05; P5: **<
324 0.01) (Fig. 3D). This suggests that the decrease in cardiomyocyte density may be linked to an
325 increase in cell death consistent with atrophy of the heart.
326
327 **Oxidative Stress is Present in SMA Hearts**
328
329 Increased apoptosis in cardiomyocytes was investigated further by examining a common
330 trigger: oxidative stress, which is present in Δ7 SMA mice exhibiting a neuromuscular
331 phenotype (Shababi *et al.,* 2010). We analysed angiotensin II receptor 1 (AT1) levels as a
332 marker of oxidative stress in the heart, as this increases ROS by elevating the activity of
333 NADPH oxidase during heart failure (Qin *et al.,* 2005). Immunohistochemistry showed
334 dramatically increased amounts of AT-1 in the SMA heart at birth compared to the control
335 heart (Fig4A). Western blot analyses confirmed these higher levels of AT-1 in SMA compared
336 to control hearts at both P3 and P5 (P1: ns > 0.05; P3: *< 0.05; P5: ** < 0.01) (Fig. 4A),
337 indicating the presence of oxidative stress in SMA hearts with onset at a pre-symptomatic
338 age.

339

340   To substantiate this finding we looked for evidence of mitochondrial-derived oxidative
341   stress as multiple proteins in the mitochondria are associated with increased ROS
342   production (Martínez-Reyes and Cuezva, 2014). This includes the ATP synthase complex,
343   which interacts directly with SMN (Fuller *et al.,* 2016). We analysed levels of subunit 6 of the
344   ATP synthase complex as mutations or overexpression of this subunit are particularly
345   associated with oxidative stress (Manczak *et al.,* 2005; Jonckheere *et al.,* 2012). Western
346   blot analyses showed significantly higher levels of MT-ATP6 in SMA at birth compared to
347   controls (P1: *<0.05) (Fig. 4B).
348   The presence of increased oxidative stress at birth not only suggests this is an important
349   event in the aetiology of SMA heart pathology, but is also indicative of early mitochondrial
350   dysfunction. As oxidative stress is present prior to increased caspase-3 expression, and
351   significantly occurs prior to the appearance of neuromuscular symptoms, it is likely to
352   precede and contribute to cardiomyocyte apoptosis and heart dysfunction.

353

354   **SMA Heart Microvasculature is Significantly Decreased**

355

356   A reduction in capillary density has been reported across multiple tissues in SMA patients
357   and animal models, where it is associated with tissue hypoxia (Somers *et al.,* 2016).
358   Previously, decreased microvasculature in the heart of the Δ7 SMA mouse model has only
359   been studied at a late-symptomatic age. Here, microvasculature was analysed at early- and
360   pre-symptomatic ages to establish if it might contribute to, rather than be a symptom of,
361   heart pathology. Immunostaining of hearts with GSL-1 endothelial cell marker indicated a
362   gross decrease in microvasculature density throughout the heart wall particularly at P5 in
363   SMA (Fig 5A,B). Western blot for a second endothelial cell marker, PECAM-1 as used
364   previously (Somers *et al*., 2012; Somers *et al.,* 2016), confirmed a significantly decreased
365   expression in SMA heart at an early-symptomatic age (P5) (P1: ns > 0.05; P3: ns > 0.05; P5:
366   *< 0.05) (Fig. 5C). This decrease in heart wall microvasculature was particularly apparent at
367   high magnification in the wall immediately adjacent to the ventricular lumen (Fig 5B). This
368   early contributing factor to cardiac defects, is likely to result in hypoxia of cardiomyocytes,
369   similar to that seen at P5 in the spinal cord of the SMA mouse, and may exacerbate
370   increased cell death.

371

372   **SMA Hearts are Congested with Blood**

373

374   The hearts used in this study were not perfused prior to fixation. Therefore, residual blood
375   left in the heart after removal is likely a reflection of functional circulatory conditions. In our
376   initial observations of histologically stained hearts, it was apparent that SMA hearts
377   contained more blood than the controls (Fig 1C). To further examine this increase, we
378   stained RBCs with Ly76 (which labels all cells in the erythrocyte lineage including RBCs). Ly76
379   marker showed that heart chambers viewed in cross-sections of P5 control hearts have only
380   small amounts of blood, whereas SMA hearts are congested with blood, which is most
381   apparent in the ventricles (Fig 6A). Quantification of Ly76 stain showed a significant (2-3
382   fold) increase in the RBCs in SMA hearts at both pre- and early-symptomatic ages compared
383   to controls (P1: ns > 0.05; P3: *< 0.05; P5: *< 0.05) (Fig 6B). This is consistent with a model
384   where the structural and molecular defects previously observed impact negatively on heart
385   function, resulting in blood pooling.

386
387

Discussion

389
390 Here, we show that Taiwanese SMA mouse hearts have thinner muscular walls, with
391 disorganised basement membranes and cardiomyocytes present pre-symptomatically.
392 Cardiomyocytes were decreased in density, likely due to increased apoptosis, at an early-
393 symptomatic age; which is associated with increased oxidative stress from birth, and also
394 decreased microvasculature in the heart at an early symptomatic age. This demonstrates
395 that heart defects are an early and important feature of disease pathogenesis in SMA.
396
397 The decrease in IVS and LV wall width described here is consistent with findings from other
398 mouse models, and may be linked to congenital heart defects such as septal defects
399 between both atria and ventricles in SMA patients. IVS thinning was present from 3 days
400 postnatally, suggesting a failure to adapt to the radical pressure changes that occur after
401 birth (Rein *et al.,* 1987). LV wall thinning was observed pre-symptomatically at birth, likely
402 affecting heart function and therefore systemic blood flow. Taken together, these findings
403 point toward impaired development of the SMA heart as a significant contributor to
404 cardiovascular defects.
405
406 *Enlarged ventricles contribute to heart dysfunction in SMA hearts*
407 Enlargement of the ventricles is commonly linked to dilation and dysfunction of the heart,
408 particularly in combination with thinning of the heart walls (Redfield *et al.,* 2003). This is
409 consistent with the cardiac phenotype described here in SMA, where dilation of the
410 ventricles is a secondary event, occurring at P3 after the primary event of a decrease in LV
411 wall width at P1. This dilation phenotype correlates with previous studies showing a
412 decreased ejection fraction in mouse SMA hearts (Bevan *et al.,* 2010; Bogdanik *et al.,* 2015),
413 and with cardiac defects, including dilation of atria and ventricles, diastolic dysfunction and
414 ventricular overload seen in SMA patients (Collado-Oritz et al., 2007; Tanaka et al., 1976;
415 Kimura et al., 1980; Distefano et al., 1994; Elkohen et al., 1996; Finsterer et al., 1999; Menke
416 et al., 2008; Kuru et al., 2009; Grotto et al., 2016). Taken together, thinning of the walls and
417 enlargement of the ventricles in the SMA heart is strikingly similar to dilated
418 cardiomyopathy (DCM), where the heart becomes enlarged and cannot pump blood
419 efficiently, evidenced by blood pooling. These defects will likely result in systolic heart
420 failure (Maron *et al.,* 2006), which has been reported in some SMA patients (Collado-Oritz et
421 al., 2007).
422
423 *Cardiomyocytes are disorganised in SMA hearts*
424 Our findings suggest that gross abnormalities in the SMA heart are underpinned by cellular
425 defects, likely driven by SMN depletion in the cardiomyocytes. Collagen IV levels were
426 decreased in SMA, likely affecting cardiomyocyte organisation through its role in basement
427 membrane structure (Lundgren *et al.,* 1988). The basement membrane maintains
428 cardiomyocyte shape (Lundgren *et al.,* 1988); anchors them to the ECM (Zellner *et al.,*
429 1991); regulates their electrical properties (Frank *et al.,* 1977; Yang *et al.,* 2014); regulates
430 sarcomeric formation and remodelling (Ross and Borg, 2001; Yang *et al.,* 2015) and

431   influences force production (Factor and Robinson, 1988; Yang *et al.,* 2015). Specifically, the
432   collagen IV network increases rigidity and strength resulting in a more fluid and powerful
433   contraction (Bruggink *et al.,* 2007).
434   This defective basement membrane and abnormal organisation of cardiomyocytes will likely
435   impair electrical conduction through end to end gap junctions (Zellner *et al.,* 1991),
436   preventing a coherent contraction to flow through the heart (Greenbaum *et al.,* 1981;
437   Sedmera and McQuinn, 2009). In addition, trabeculae are more common in SMA hearts and
438   the cardiac muscle is circumferentially rather than spirally oriented, both of which suggest
439   that the heart wall is not maturing correctly in the embryonic period. Compaction of
440   trabeculae contributes to the thickness of the ventricular and IVS muscular mass, the
441   papillary muscles, vasculature and the conduction system (Sedmera *et al.*, 2000). The failed
442   compaction seen in the SMA heart may underlie septal defects and arrhythmias seen in SMA
443   patients.
444
445   *Oxidative stress is present in SMA hearts*
446   In parallel with the structural defects described above, the pre-symptomatic increases in AT-
447   1 and MT-ATP6 reported here suggest that oxidative stress is present in the SMA heart, and
448   that it precedes increased cardiomyocyte death. Oxidative stress is thought to be critical for
449   the activation of apoptosis, including caspase activation, in failing hearts (Cesselli *et al.,*
450   2001). AT-1 is also increased in the heart of the Δ7 SMA mouse model (Shababi *et al.,* 2010),
451   which points to oxidative stress as a common mechanism in SMA cardiovascular pathology.
452   In our study caspase levels do not correlate perfectly with cardiomyocyte density, which is
453   likely due to the high variability in proliferation of cardiomyocytes, particularly at P3,
454   contributing to the decrease in cell number prior to the increase in cell death.
455
456   As ATP synthase subunits interact directly with SMN protein, and are overexpressed in the
457   CNS of multiple SMA models, there is a potentially direct mechanistic link between SMN
458   depletion and cardiac dysfunction (Fuller *et al.* 2016). Taken further, defects in
459   mitochondria, including fragmentation of the mitochondrial network, impaired
460   mitochondrial membrane potential and increased oxidative stress are all thought to be
461   associated with motor neurone cell death in SMA (Acsadi *et al.,* 2009; Ripolone *et al.,* 2015;
462   Miller *et al.,* 2016; Xu *et al.,* 2016; Boyd *et al.,* 2017). Cardiomyocytes contain many
463   mitochondria (more than skeletal muscle) to support their high-energy demands (Hom and
464   Sheu, 2009), and are therefore highly susceptible to mitochondrial dysfunction-mediated
465   oxidative stress. Swollen and degenerating mitochondria are seen in cardiomyocytes in late-
466   symptomatic SMNΔ7 mice (Bevan *et al.,* 2010), which is consistent with late-stage heart
467   failure. Here, however, we show that the changes in the level of a mitochondrial specific
468   protein, MT-ATP6 are already present at birth suggesting that mitochondrial dysfunction
469   may be a primary driver of cardiac defects in SMA.
470
471   *Blood pools in the ventricls of SMA hearts*

472   The thin heart walls in SMA are likely to contract less efficiently, resulting in a decreased
473   ejection fraction (Bevan *et al.,* 2010; Bogdanik *et al.,* 2015), blood pooling (Ghio *et al.,*
474   2001), additional stress, increased cell death and a positive feedback loop ultimately leading
475   to heart failure (Narula *et al.,* 1996). However, the heart is a dynamic organ and abnormal
476   blood flow through the heart, altered by forces including preload and afterload (Bugge-
477   Asperheim and Kiil, 1973), could also contribute to blood pooling. In addition, extrinsic
478   factors such as altered blood composition, including that resulting from abnormal
479   erythropoiesis and platelet production in the SMA liver (Szunyogova *et al.,* 2016), will
480   impact on blood flow and contribute to ventricular distension. These alterations in blood
481   flow and observations of blood pooling could also explain the pulmonary hypertension and
482   pulmonary effusion reported in SMA patients (Møller et al., 1990; Distefano et al., 1994; El-
483   Matary et al., 2004; Menke et al., 2008). Here (see Fig. 7), we propose a model to interpret
484   the cardiac defects observed.
485
486   With a new treatment for SMA, Spinraza (Nusinersen), approved by the FDA and EMA, it is
487   now critically important to understand these cardiovascular pathologies. The drug is
488   administered intrathecally, and therefore only targets the central nervous system (Hoy *et*
489   *al.,* 2017), which appears to limit its utility in disease treatment (Finkel et al., 2017).
490   Conversely, an as yet unapproved, systemically-administered gene therapy, may offer hope
491   of obtaining significant patient benefit (Mendell et al, 2017), by treating the disease as a
492   whole. Consequently, it is an unfortunate possibility that cardiovascular defects may be
493   uncovered in these treated SMA patients.
494

Conclusion

495
496
497   In conclusion, the severe Taiwanese SMA mouse model has severe cardiac defects from
498   birth. Thinning of the IVS and dilation of ventricular lumens was seen from pre-symptomatic
499   ages through until late symptomatic stages of disease. But most significantly, changes in the
500   LV width were observed from birth, prior to motor neurone pathology. There were also
501   changes in the organisation of cardiomyocytes from birth in SMA, which may be linked to
502   altered levels of basement membrane protein collagen IV; increased oxidative stress in
503   cardiomyocytes pre-symptomatically; increased apoptosis of cardiomyocytes seen at early-
504   symptomatic ages; decreased microvasculature also at an early symptomatic age; and increased
505   blood pooling within the SMA heart ventricles at a pre-symptomatic age. This combines to
506   suggest a phenotype similar to dilated cardiomyopathy that will most likely lead to heart
507   failure. It is therefore essential to develop systemic therapies for SMA capable of treating
508   these cardiac pathologies, in addition to the well-established neuromuscular defects.
509

510   # Acknowledgements

523 ## Conflict of Interest

524

525 Please note that SHP is a member of the JoA Editorial Board and THG is joint EiC of JoA.

Author Contributions

527

528 SHP, THG, GKM and ES designed the study
529 GKM, ES and HKS carried out the experiments
530 GKM analysed the data
531 SHP, THG, GKM, ES and HKS prepared the manuscript

532 References

533

534 Acsadi, G., Lee, I., Li, X., Khaidakov, M., Pecinova, A., Parker, G. and Hüttemann, M. (2009).
535 Mitochondrial dysfunction in a neural cell model of spinal muscular atrophy. *Journal of*
536 *Neuroscience Research,* **87**(12), 2748-2756.

537 Adachi, S., Ito, H., Tamamori-Adachi, M., Ono, Y., Nozato, T., Abe, S., Ikeda, M., Marumo, F.
538 and Hiroe, M. (2001). Cyclin A/cdk2 activation is involved in hypoxia-induced apoptosis in
539 cardiomyocytes. *Circulation Reseasrch,* **89**(4), 408-414.

540 Arai, H., Tanabe, Y., Hachiya, Y., Otsuka, E., Kumada, S., Furushima, W., Kohyama, J.,
541 Yamashita, S., Takanashi, J. and Kohno, Y. (2005). Finger cold-induced vasodilation,
542 sympathetic skin response and R-R interval variation in patients with progressive spinal
543 muscular atrophy. *Journal of Child Neurology*, **20**(11), 871-875.

544 Araujo, A., Araujo, M. and Swoboda, K. (2009). Vascular perfusion abnormalities in infants
545 with spinal muscular atrophy. *Journal of Pediatrics*, **155**(2), 292-294.

546 Bevan, A., Hutchinson, K., Foust, K., Braun, L., McGovern, V., Schmelzer, L., Ward, J.,
547 Petruska, J., Lucchesi, P., Burghes, A. and Kasper, B. (2010). Early heart failure in the SMN Δ7
548 model of spinal muscular atrophy and correction by postnatal scAAV9-SMN delivery. *Human*
549 *Molecular Genetics,* **19**(20), 3895-3905.

550 Biondi, O., Lopes, P., Desseille, C., Branchu, J., Chali, F., Salah, A., Pariset, C., Chanoine, C.
551 and Charbonnier, F. (2012). Physical exercise reduces cardiac defects in type 2 spinal
552 muscular atophy-like mice. *Journal of Physiology,* **590**(22), 5907-5925.

553 Bogdanik, L., Osborne, M., Davis, C., Martin, W., Austin, A., Rigo, F., Bennett, C. and Lutz, C.
554 (2015). Systemic, postsymptomatic antisense oligonucleotide rescues motor unit maturation
555 delay in a new mouse model for type II/III spinal muscular atrophy. *Proceeding of the*
556 *National Academy of Sciences of the United States of America,* **112**(43), 865-872.

557 Bowerman, M., Michalski, J., Beauvais, A., Murray, L., De Repentigny, Y. and Kothary, R.
558 (2014). Defects in pancreatic development and glucose metabolism in SMN-depleted mice
559 independent of canonical spinal muscular atrophy neuromuscular pathology. *Human*
560 *Molecular Genetics,* **23**(13), 3432-3444.

561 Bowerman, M., Swoboda, K., Michalski, J., Wang, G., Reeks, C., Beauvais, A., Murphy, K.,
562 Woulfe, J., Screaton, R., Scott, F. and Kothary, R. (2012). Glucose metabolism and pancreatic
563 defects in spinal muscular atrophy. *Annals of Neurology,* **72**(2), 256-268.

564 Boyd, P., Tu, W., Shorrock, H., Groen, E., Carter, R., Powis, R., Thomson, S., Thomson, D.,
565 Graham, L., Motyl, A., Wishart, T., Highley, J., Morton, N., Becker, T., Becker, C., Heath, P.
566 and Gillingwater, T. (2017). Bioenergetic status modulates motor neuron vulnerability and

567   pathogenesis in a zebrafish model of spinal muscular atrophy. *PLOS Genetics,* **13**(4),
568   e1006744.

569   Bruggink, A., Van Oosterhout, M., De Jonge, N., Cleutjens, J., Van Wichen, D., Van Kuik, J.,
570   Tilanus, M., Gmelig-Meyling, F., Van Den Tweel, J. and De Wenger, R. (2007). Type IV
571   collagen degradation in the myocardial basement membrane after unloading of the failing
572   heart by a left ventricular assist device. *Laboratory Investigation,* **87**(11), 1125-1137.

573   Bugge-Asperheim, B. and Kiil, F. (1973). Preload, contractility, and afterload as determinants
574   of stroke volume during elevation of aortic blood pressure in dogs. *Cardiovascular Research,*
575   **7**(4), 328-341.

576   Buja, M. and Entman, M. (1998). Modes of myocardial cell injury and cell death in ischemic
577   heart disease. *Circulation,* **98**(14), 1355-1357.

578   Bürglen, L., Spiegel, R., Ignatius, J., Cobben, J., Landrieu, P., Lefebvre, S., Munnich, A. and
579   Melki, J. (1995). SMN gene deletion in variant of infantile spinal muscular atrophy. *The
580   Lancet*, **346**(8970), 316-317.

581   Catapano, F., Zaharieva, I., Scoto, M., Marrosu, E., Morgan, J., Muntoni, F. and Zhou, H.
582   (2016). Altered levels of microRNA-9, -206, and -132 in spinal muscular atrophy and their
583   response to antisense oligonucleotide therapy. *Molecular Therapy – Nucleic Acids,* **5**(7),
584   e331.

585   Cesselli, D. Jakoniuk, I., Barlucchi,L., Beltrami, A., Hintze, T., Nadal-Ginard, B., Kajstura, J.,
586   Leri, A. and Anversa, P. (2001). Oxidative stress-mediated cardiac cell death is a major
587   determinant of ventricular dysfunction and failure in dog dilated cardiomyopathy.
588   *Circulation Research,* **89**(3), 279-286.
589
590   Collado-Ortiz, M., Shkurovich-Bialik, P., González-De Leo, S. ad Arch-Tirado, E. (2007). Type 1
591   spinal atrophy (Werdnig-Hoffman disease). Case report. *Cirugia y Cirujanos*, **75**(2), 119-122.

592   Coletta, C., Carboni, P., Carunchio, A., Porro, G. and Bacci, V. (1989). Electrocardiographic
593   abnormalities in childhood spinal muscular atrophy. *International Journal of Cardiology,*
594   **24**(3), 283-288.

595   Cook, A., Curzon, C. and Milazzo, A. (2006). An infant with hypoplastic left heart syndrome
596   and spinal muscular atrophy. *Cardiology in the Young,* **16**(1), 78-80.

597   Dawood, A. and Moosa, A. (1983). Hand and ECG tremor in spinal muscular atrophy.
598   *Archives of Disease in Childhood,* **58**(5), 376-378.

599   Deguise, M., De Repentigny, Y., McFall, E., Auclair, N., Sad, S. and Kothary, R. (2017).
600   Immune dysregulation may contribute to disease pathogenesis in spinal muscular atrophy
601   mice. *Human Molecular Genetics*, **26**(4), 801-819.

602   Distefano, G., Sciacca, P., Parisi, M., Parano, E., Smilari, P., Marietta, M. and Fiumara, A.
603   (1994). Heart involvement in progressive spinal muscular atrophy. A review of the literature
604   and case histories in childhood. *Pediatria Medica Chirurgica*, **16**(2), 125-128.

605   Eaton, S., Hurtado, M., Oldknow, K., Graham, L., Marchant, T., Gillingwater, T., Farquharson,
606   C. and Wishart, T. (2014). A guide to modern quantitative fluorescent western blotting with
607   troubleshooting strategies. *Journal of Visualized Experiments*, **93**, e52099.

608   Eaton, S., Roche, S., Hurtado, M., Oldknow, K., Farquharson, C., Gillingwater, T. and Wishart,
609   T. (2013). Total protein analysis as a reliable loading control for quantitative fluorescent
610   western blotting. *PLOS One*, **8**(8), e72457.

611   El-Matary, W., Kotagiri, S., Cameron, D. and Peart, I. (2004). Spinal muscle atrophy type 1
612   (Werdnig-Hoffman disease) with complex cardiac malformation. *European Journal of
613   Pediatrics,* **163**(6), 331-332.

614   Elkohen, M., Vaksmann, G., Elkohen, M., Francart, C., Foucher, C. and Rey, C. (1996). Cardiac
615   involvement in Kugelberg-Welander disease: A prospective study of 8 cases. *Archives des
616   Maladies du Coeur et des Vaisseaux,* **89**(5), 611-617.

617   Factor, S. and Robinson, T. (1988). Comparative connective tissue structure-function
618   relationships in biological pumps. *Lab Investigations,* **58**(2), 150-156.

619   Finkel, R., Mercuri, E., Darras, B., Connolly, A., Kuntz, N., Kirschner, J., Chiriboga, C., Saito, K.,
620   Servais, L., Tizzano, E., Topaloglu, H., Tulinius, M., Montes, J., Glanzman, A., Bishop, K.,
621   Zhong, Z., Gheuens, S., Bennett, C., Schneider, E., Farwell, W. and De Vivo, D. (2017).
622   Nusinersen versus sham control in infantile-onset spinal muscular atrophy. *The New
623   England Journal of Medicine,* **377**(18), 1723-1732.

624   Finsterer, J. and Stöllberger, C. (1999) Cardiac involvement in Werdnig-Hoffmann's spinal
625   muscular atrophy. *Cardiology,* **92**(3), 178-182.

626   Frank, J., Langer, G., Nudd, L. and Seraydarian, K. (1977). The myocardial cell surface, its
627   histochemistry, and the effect of sialic acid and calcium removal on its structure and cellular
628   ionic exchange. *Circulation Research,* **41**(5), 702-714.

629   Fuller, H., Gillingwater, T. and Wishart, T. (2016). Commonality amid diversity: Multi-study
630   proteomic identification of conserved disease mechanisms in spinal muscular atrophy.
631   *Neuromuscular Disorders,* **26**(9), 560-569.

632   Gardner-Medwin, D., Hudgson, P. and Walton, J. (1967). Benign spinal muscular atrophy
633   arising in childhood and adolescence. *Journal of the Neurological Sciences,* **5**(1), 121-158.

634   Ghio, S., Gavazzi, A., Campana, C., Inserra, C., Klersy, C., Sebastiani, R., Arbustini, E.,
635   Recusani, F. and Tavazzi, L. (2001). Independent and additive prognostic value of right

636   ventricular systolic function and pulmonary artery pressure in patients with chronic heart
637   failure. *Journal of the American College of Cardiology,* **37**(1), 183-188.

638   Gogliotti, R., Quinlan, K., Barlow, C., Heier, C., Heckman, C. and DiDonato, C. (2012). Motor
639   neuron rescue in spinal muscular atrophy mice demonstrates that sensory-motor defects
640   are a consequence, not a cause, of motor neuron dysfunction. *Journal of Neuroscience,*
641   **32**(11), 3818-3829.

642   Greenbaum, R., Ho, S., Gibson, D., Becker, A. and Anderson, R. (1981). Left ventricular fibre
643   architecture in man. *British Heart Journal,* **45**(3), 248-263.

644   Grotto, S., Cuisset, J., Marret, S., Drunat, S., Faure, P., Audebert-Bellanger, S., Desguerre,
645   I., Flurin, V., Grebille, A., Guerrot, A., Journel, H., Morin, G., Plessis, G., Renolleau, S., Roume,
646   J., Simon-Bouy, B., Touraine, R., Willems, M., Frébourg, T., Verspyck, E., Saugier-Veber, P.
647   (2016). Type 0 spinal muscular atrophy: Further delineation of prenatal and postnatal
648   features in 16 patients. *Journal of Neuromuscular Diseases*, **3**(4), 487-495.

649   Hachiya, Y., Arai, H., Hayashi, M., Kumada, S., Furushima, W., Ohtsuka, E., Ito, Y., Uchiyama,
650   A. and Kurata, K. (2005). Autonomic dysfunction in cases of spinal muscular atrophy type 1
651   with long survival. *Brain and Development,* **27**(8), 574-578.

652   Haliloglu, G., Gungor, M. and Anlar, B. (2015). The role of electrocardiography in the
653   diagnosis of spinal muscular atrophy type III. *The Journal of Pediatrics,* **166**(4), 1092.

654   Hamilton, G. and Gillingwater, T. (2013). Spinal muscular atrophy: Going beyond the motor
655   neuron. *Trends in Molecular Medicine,* **19**(1), 40-50.

657   Heier, C., Satta, R., Lutz, C. and Didonato, C. (2010). Arrhythmia and cardiac defects are a
658   feature of spinal muscular atrophy model mice. *Human Molecular Genetics,* **19**(20), 3906-
659   3918.

660   Hoffmann, J. (1892). Familial spinal muscular atrophy in infancy. *Dtsch Z Nervenheilkd,* **3**,
661   427-470.

662   Hom, J., Sheu, S. (2009). Morphological dynamics of mitochondria – A special emphasis on
663   cardiac muscle cells. *Journal of Molecular and Cellular Cardiology,* **46**(6), 811-820.

664   Hoy, S. (2017). Nusinersen: First global approval. *Drugs,* **77**(4), 473-479.

665   Hsieh-Li, H., Chang, J., Jong, Y., Wu, M., Wang, N., Tsai, C. and Li, H. (2000). A mouse model
666   for spinal muscular atrophy. *Nature Genetics,* **24**(1), 66-70.

667   Hua, Y., Liu, Y., Sahashi, K., Rigo, F., Bennett, C. and Krainer, A. (2015) Motor neuron cell-
668   nonautonomous rescue of spinal muscular atrophy phenotypes in mild and severe
669   transgenic mouse models. *Genes and Development,* **29**(3), 288-297.

670   Hua, Y., Sahashi, K., Rigo, F., Hung, G., Horev, G., Bennett, C. and Krainer, A. (2011).
671   Peripheral SMN restoration is essential for long-term rescue of a
672   severe spinal muscular atrophy mouse model. *Nature*, **478**(7367), 123-126.

673   Jonckheere, A., Smeitink, J. and Rodenburg, R. (2012). Mitochondrial ATP synthase:
674   Architecture, function and pathology. *Journal of Inherited Metabolic Disease,* **35**(2), 211-
675   225.

676   Jong, Y., Chang, J. and Wu, J. (1998). Large-scale deletions in a Chinese infant associated
677   with a variant form of Werdnig-Hoffmann disease. *Neurology*, **51**(3), 878-879.

678   Khairallah, M., Astroski, J., Custer, S., Androphy, E., Franklin, C. and Lorson, C. (2017). SMN
679   deficiency negatively impacts red pulp macrophages and spleen development in mouse
680   models of spinal muscular atrophy. *Human Molecular Genetics*, **26**(5), 932-941.

681   Kimura, S., Yokota, H., Tateda, K., Miyamoto, K., Yamamoto, K., Shibata, J. (1980). A case of
682   the Kugelberg-Welander syndrome complicated with cardiac lesions. *Japanese Heart*
683   *Journal,* **21**(3), 417-422.

684   Krupickova, S., Rigby, M., Jicinska, H., Marais, G., Rubens, M. and Carvalho, J. (2017). Total
685   anomalous pulmonary venous connection to an unroofed coronary sinus diagnosed in a
686   fetus with associated spinal muscular atrophy type I. *Ultrasound in Obstetrics and*
687   *Gynecology,* uog. 17432**.**

688   Kuru, S., Sakai, M., Konagaya, M., Yoshida, M., Hashizume, Y. and Saito, K. (2009). An
689   autopsy case of spinal muscular atrophy type III (Kugelberg-Welander disease).
690   *Neuropathology,* **29**(1), 63-67.

691   Lefebvre, S., Bürglen, L., Reboullet, S., Clermont, O., Burlet, P., Viollet, L., Benichou, B.,
692   Cruaud, C., Millasseau, P., Zeviani, M., Le Paslier, D., Frézal, J., Cohen, D., Weissenbach, J.,
693   Munnich, A. and Melki. (1995). Identification and characterisation of a spinal muscular
694   atrophy-determining gene. *Cell,* **80**(1), 155-156.

695   Lorson, C., Hahnen, E., Androphy, E. and Wirth, B. (1999). A single nucleotide in the SMN
696   gene regulates splicing and is responsible for spinal muscular atrophy. *Proceedings of the*
697   *National Academy of Sciences*, **96**(11), 6307-6311.

698   Lundgren, E., Gullberg, D., Rubin, K., Borg, T., Terracio, M. and Terracio, L. (1988). In vitro
699   studies on adult cardiac myocytes: Attachment and biosynthesis of collagen IV and laminin.
700   *Journal of Cellular Physiology,* **136**(1), 43-53.

701   Lunn, M. and Wang, C. (2008). Spinal muscular atrophy. *The Lancet,* **371**(9630), 2120-2133.

702   Manczak, M., Jung, Y., Park, B., Partovi, D. and Reddy, P. (2005). Time-course of
703   mitochondrial gene expressions in mice brains: implications for mitochondrial dysfunction,
704   oxidative damage, and cytochrome c in aging. *Journal of Neurochemistry,* **92**(3), 494-504.

705

Maron, B., Towbin, J. Thiene, G., Antzelevitch, C., Corrado, D., Arnett, D., Moss, A., Seidman, C. and Young, J. (2006). An American Heart Association scientific statement from the council on clinical cardiology, heart failure and transplantation committee; quality of care and outcomes research and functional genomics and translational biology interdisciplinary working groups; and council on epidemiology and prevention. *Circulation,* **113**(14), 1807-1816.

Martínez-Reyes, I. and Cuezva, J. (2014). The H⁺-ATP synthase: A gate to ROS-mediated cell death or cell survival. *Biochimica et Biophysica Acta – Bioenergetics,* **1837**(7), 1099-1112.

Mendell, J., Al-Zaidy, S., Shell, R., Arnold, W., Rodino-Klapac, L., Prior, T., Lowes, L., Alfano, L., Berry, K., Church, K., Kissel, J., Nagendran, S., L'Italien, J., Sproule, D., Wells, C., Cardenas, J., Heitzer, M., Kaspar, A., Corcoran, S., Braun, L., Likhite, S., Miranda, C., Meyer, K., Foust, K., Burghes, A. and Kaspar, B. (2017). Single-dose gene-replacement therapy for spinal muscular atrophy. *The New England Journal of Medicine,* **377**(18), 1713-1722.

Menke, L., Poll-The, B., Clur, S., Bilardo, C., Van Der Wal, A., Lemmink, H. and Cobben, J. (2008). Congenital heart defects in spinal muscular atrophy type I: A clinical report of two siblings and a review of the literature. *American Journal of Medical Genetics, Part A,* **146**(6), 740-744.

Miller, N., Shi, H., Zelikovich, A. and Ma, Y. (2015). Motor neuron mitochondrial dysfunction in spinal muscular atrophy. *Human Molecular Genetics,* **25**(16), 3395-3406.

Møller, P., Moe, N., Saugstad, O., Skullerud, K., Velken, M., Berg K, Nitter-Hauge, S and Børresen, A. (1990) Spinal muscular atrophy type 1 combined with atrial septal defect in three sibs. *Clinical Genetics.* **38**(2), 81-83.

Mulleners, W., Van Ravenswaay, C., Gabreels, F., Hamel, B., Van Oort, A. and Sengers, R. (1996). Spinal muscular atrophy combined with congenital heart disease: A report of two cases. *Neuropediatrics,* **27**(6), 333-334.

Narula, J., Haider, N., Virmani, R., Disalvo, T., Kolodgie, F., Hajjar, R., Schmidt, U., Semigran, M., Dec, G. and Khaw, B. (1996). Apoptosis in myocytes in end-stage heart failure. *New England Journal of Medicine,* **335**(16), 1182-1189.

Narver, H., Kong, L., Burnett, B., Choe, D., Bosch-Marcé, M., Taye, A., Eckhaus, M. and Sumner, C. (2008). Sustained improvement of spinal muscular atrophy mice treated with trichostatin A plus nutrition. *Annals of Neurology,* **64**(4), 465-470.

Nash, L., Burns, J., Chardon, J., Kothary, R. and Parks, R. (2016). Spinal muscular atrophy: More than a disease of motor neurons? *Current Molecular Medicine,* **16**(9), 779-792.

739 Ottesen, E., Howell, M., Singh, N., Seo, J., Whitley, E. and Singh, R. (2016). Severe
740 impairment of male reproductive organ development in a low SMN expressing mouse
741 model of spinal muscular atrophy. *Scientific Reports,* **6**, 20193.

742 Porter, A. and Jänicke, R. (1999) Emerging roles of caspase-3 in apoptosis. *Cell Death and*
743 *Differentiation,* **6**(2), 99-104.

744 Powis, R. and Gillingwater, T. (2016a). Selective loss of alpha motor neurons with sparing of
745 gamma motor neurons and spinal cord cholinergic neurons in a mouse model of spinal
746 muscular atrophy. *Journal of Anatomy,* **228**(3), 443-451.

747 Powis, R., Karyka, E., Boyd, P., Côme, J., Jones, R., Zheng, Y., Szunyogova, E., Groen, E.,
748 Hunter, G., Thomson, D., Wishart, T., Becker, C., Parson, S., Martinat, C., Azzouz, M. and
749 Gillingwater, T. (2016b). Systemic restoration of UBA1 ameliorates disease in spinal
750 muscular atrophy. *JCI Insight,* **1**(11), e87908.

751 Qin, F., Patel, R., Yan, C. and Weimin, L. (2005). NADPH oxidase is involved in angiotensin II-
752 induced apoptosis in H9C2 cardiac muscle cells: Effects of apocynin. *Free Radical Biology*
753 *and Medicine,* **40**(2), 236-246.

754 Redfield, M., Jacobsen, S., Burnett, J., Mahoney, D., Bailey, K. and Rodeheffer, R. (2003).
755 Burden of systolic and diastolic ventricular dysfunction in the community: Appreciating the
756 scope of the heat failure epidemic. *Journal of the American Medical Association,* **289**(2),
757 194-202.

758 Rein, A., Sanders, S., Colan, S., Parness, I. and Epstein, M. (1987). Left ventricular mechanics
759 in the normal newborn. *Circulation,* **76**(5), 1029-1036.

760 Riessland, M., Ackermann, B., Förster, A., Jakubik, M., Hauke, J., Garbes, L., Fritzsche, I.,
761 Mende, Y., Blumcke, I., Hahnen, W. and Wirth, B. (2010). SAHA ameliorates the SMA
762 phenotype in two mouse models for spinal muscular atrophy. *Human Molecular Genetics,*
763 **19**(8), 1492-1506.

764 Ripolone, M., Ronchi, D., Violano, R., Vallejo, D., Fagiolari, G., Barca, E., Lucchini, V.,
765 Colombo, I., Villa, L., Berardinelli, A., Balottin, U., Morandi, L., Mora, M., Bordoni, A.,
766 Fortunato, F., Corti, S., Parisi, D., Toscano, A., Sciacco, M., Di Mauro, S.,, Comi, G. and
767 Moggio, M. (2015). Impaired muscle mitochondrial biogenesis and myogenesis in spinal
768 muscular atrophy. *JAMA Neurology*, **72**(6), 666-675.
769
770 Roos, M., Sarkozy, A., Chierchia, G., De Wilde, P., Schmedding, E. and Brugada, P. (2009).
771 Malignant ventricular arrhythmia in a case of adult onset of spinal muscular atrophy
772 (Kugelberg-Welander disease). *Journal of Cardiovascular Electrophysiology,* **20**(3), 342-344.
773

774   Ross, R. and Borg, T. (2001). Integrins and the myocardium. *Circulation Research,* **88**(11),
775   1112-1119.

776   Rudnik-Schöneborn, S., Heller, R., Berg, C., Betzler, C., Grimm, T., Eggermann, T.,
777   Eggermann, K., Wirth, R., Wirth, B. and Zerres, K. (2008). Congenital heart disease is a
778   feature of severe infantile spinal muscular atrophy. *Journal of Medical Genetics*, **45**(10), 635-
779   638.

780   Rudnik-Schöneborn, S., Vogelgesang, S., Armbrust, S., Graul-Neumann, L., Fusch, C. and
781   Zerres, K. (2010). Digital necroses and vascular thrombosis in severe spinal muscular
782   atrophy. *Muscle and Nerve,* **42**(1), 144-147.

783   Sarnat, H. and Trevenen, C. (2007). Motor neuron degeneration in a 20-week male fetus:
784   spinal muscular atrophy type 0. *Canadian Journal of Neurological Sciences,* **34**(2), 215-220.

785   Scholzen, T. and Gerdes, J. (2000). The Ki-67 protein: From the known and the unknown.
786   *Journal of Cellular Physiology,* **182**(3), 311-322.

787   Schreml, J., Riessland, M., Paterno, M., Garbes, L., Roßbach, K., Ackermann, B., Krämer,
788   J., Somers, E., Parson, S., Heller, R., Berkessel, A., Sterner-Kock, A. and Wirth, B. (2013).
789   Severe SMA mice show organ impairment that cannot be rescued by therapy with the
790   HDACi JNJ-26481585. *European Journal of Human Genetics,* **21**(6), 643-652.

791   Sedmera, D. and McQuinn, T. (2008). Embryogenesis of the heart muscle. *Heart Failure*
792   *Clinics,* **4**(3), 235-245.

793   Sedmera, D., Pexieder, T., Vuillemin, M., Thompson, R. and Anderson, R. (2000).
794   Developmental patterning of the myocardium. *Anatomical Record,* **258**(4), 319-337.

795   Shababi, M., Habibi, J., Ma, L., Glascock, J., Sowers, J. and Lorson, C. (2012). Partial
796   restoration of cardio-vascular defects in a rescued severe model of spinal muscular atrophy.
797   *Journal of Molecular and Cellular Cardiology*, **52**(5), 1074-1082.

798   Shababi, M., Habibi, J., Yang, H., Vale, S., Sewell, W. and Lorson, C. (2010). Cardiac defects
799   contribute to the pathology of spinal muscular atrophy models. *Human Molecular Genetics,*
800   **19**(20), 4059-4071.

801   Shababi, M., Lorson, C. and Rudnik-Schöneborn, S. (2014). Spinal muscular atrophy: a motor
802   neuron disorder or a multi-organ disease? *Journal of Anatomy*, **224**(1), 15-28.
803
804   Sintusek, P., Catapano, F., Angkathunkayul, N., Marrosu, E., Parson, S., Morgan, J., Muntoni,
805   F. and Zhou, H. (2016). Histopathological defects in intestine in severe spinal muscular
806   atrophy mice are improved by systemic antisense oligonucleotide treatment. *PLOS One,*
807   **11**(5), e0155032.

808   Somers, E., Lees, R., Hoban, K., Sleigh, J., Zhou, H., Muntoni, F., Talbot, K., Gillingwater, T.
809   and Parson, S. (2016). Vascular defects and spinal cord hypoxia in spinal muscular atrophy.
810   *Annals of Neurology,* **79**(2), 217-230.

811   Somers, E., Stencel, Z., Wishart, T., Gillingwater, T. and Parson, S. (2012). Density, calibre
812   and ramification of muscle capillaries are altered in a mouse model of severe spinal
813   muscular atrophy. *Neuromuscular Disorders*, **22**(5), 435-442.

814   Sterne, J. and Lavieuville, M. (1964). Cardiac manifestations during diseases of the nervous
815   and muscular systems. *Gazette Médicale de France,* **71**, 1925-1932.

816   Szunyogova, E., Zhou, H., Maxwell, G., Powis, R., Muntoni, F., Gillingwater, T. and Parson, S.
817   (2016). Survival Motor Neuron (SMN) protein is required for normal
818   mouse liver development. *Scientific Reports,* **6**, 34635

819   Takahashi, N., Shimada, T., Ishibashi, Y., Sugamori, T., Hirano, Y., Oyake, N. and Murakami, Y.
820   (2006). Cardiac involvement in Kugelberg-Welander disease: A case report and review.
821   *American Journal of the Medical Sciences,* **332**(6), 354-356.

822   Tanaka, H., Nishi, S., Nuruki, K., Tanaka, N. (1977). Myocardial ultrastructural changes in
823   Kugelberg-Welander syndrome. *British Heart Journal,* **39**(12), 1390-1393.

824   Tanaka, H., Uemura, N., Toyama, Y., Kudo, A. and Ohkatsu. (1976). Cardiac involvement in
825   the Kugelbert-Welander syndrome. *American Journal of Cardiology,* **38**(4), 528-532.

826   Thomson, A., Somers, E., Powis, R., Shorrock, H., Murphy, K., Swoboda, K., Gillingwater, T.
827   and Parson, S. (2016). Survival of motor neuron protein is required for normal postnatal
828   development of the spleen. *Journal of Anatomy,* **230**(2), 337-346.

829   Tsai, M., Chiu, Y., Wang, S., Hsieh-Li, H., Lian, W., Li, H. (2006). Abolishing bax-dependent
830   apoptosis shows beneficial effects on spinal muscular atrophy model mice. *Molecular
831   Therapy,* **13**(6), 1149-1155.

832   Vaidla, E., Talvik, I., Kulla, A., Sibul, H., Maasalu, K., Metsvaht, T., Piirsoo, A. and Talvik, T.
833   (2007). Neonatal spinal muscular atrophy type 1 with bone fractures and heart defect.
834   *Journal of Child Neurology,* **22**(1), 67-70.

835   Vitte, J., Davoult, B., Roblot, N., Mayer, M., Joshi, V., Courageot, S., Tronche, F., Vadrot, J.,
836   Moreau, M., Kemeny, F. and Melki, J. (2004). Deletion of murine Smn exon 7 directed to
837   liver leads to severe defect of liver development associated with iron overload. *The
838   American Journal of Pathology*, **165**(5), 1731-1741.

839   Werdnig, G. (1891). Two early infantile hereditary cases of progressive muscular atrophy
840   simulating dystrophy, but on a neural basis. *Archives of Psychiatric Nursing,* **22**, 437–481.

841   Wijngaarde, C., Blank, A., Stam, M., Wadman, R., Van Den Berg, L. and Van Der Pol, W.
842   (2017). Cardiac pathology in spinal muscular atrophy: a systematic review. *Orphanet Journal*
843   *of Rare Diseases*, **12**(1), 67.

844   Wishart, T., Mutsaers, X., Riessland, M., Reimer, M., Hunter, G., Hannam, M., Eaton, S.,
845   Fuller, H., Roche, S., Somers, E., Morse, R., Young, P., Lamont, D., Hammerschmidt, M.,
846   Joshi, A., Hohenstein P., Morris, G., Parson, S., Skehel, P., Becker, T., Robinson, I., Becker, C.,
847   Wirth, B. and Gillingwater, T. (2014). Dysregulation of ubiquitin homeostasis and β-catenin
848   signaling promote spinal muscular atrophy. The *Journal of Clinical Investigation*, **124**(4),
849   1821-1834.

850   Xu, C., Denton, K., Wang, Z., Zhang, X. and Li, X. Abnormal mitochondrial transport and
851   morphology as early pathological changes in human models of spinal muscular atrophy.
852   *DMM Disease Models and Mechanisms,* **9**(1), 39-49.

853   Yang, H., Borg, T., Liu, H. and Gao, B. (2015). Interactive relationship between basement-
854   membrane development and sarcomerogenesis in single cardiomyocytes. *Experimental Cell*
855   *Research,* **330**(1), 222-232.
856
857   Yang, H., Borg, T., Wang, Z., Ma, Z. and Gao, B. (2014). Role of the basement membrane in
858   regulation of cardiac electrical properties. *Annals of Biomedical Engineering,* **42**(6), 1148-
859   1157.

860   Zellner, J., Spinale, F., Eble, D., Hewett, K. and Crawford, F. (1991). Alterations in myocyte
861   shape and basement membrane attachment with tachycardia-induced heart failure.
862   *Circulation Research,* **69**(3), 590-600.

Figure Legends

Figure 1:

Gross Morphology of the Heart is Altered in SMA

(A) Representative images of early-symptomatic P5 hearts from heterozygous control and SMA disease mice. Scale bar represents 5mm. **(B)** Weight of control and SMA heart, expressed as as a % of body weight, at birth (P1), pre-symptomatic (P3), early-symptomatic (P5) and late-symptomatic ages (P8). **(C)** Transverse sections through the ventricles of early-symptomatic P5 hearts of control and SMA mice stained with H&E, LV= left ventricle, RV = right ventricle, scale bar represents 200µm. **(D)** Cross-sectional area of both ventricles, expressed as a % of total cross sectional area of heart in control and SMA mice at birth (P1), pre-symptomatic (P3) and early-symptomatic (P5) ages. **(E)** Width of interventricular septum (IVS) in relation to body weight of control and SMA mice at birth (P1), pre-symptomatic (P3) and early-symptomatic (P5) ages. **(F)** Width of LV wall in relation to body weight of control and SMA mice at birth (P1), pre-symptomatic (P3) and early-symptomatic (P5) ages. Error bars, mean ±SEM (n≥3 mice per group). A two-way ANOVA was used to calculate *p*-values.

Figure 2:

Cardiomyocytes are Disorganised in the SMA Heart

(A) Representative micrographs in control and SMA hearts, at birth (P1), pre-symptomatic (P3) and early-symptomatic (P5) ages, immunostained for collagen IV to show the basement membrane. Images show transverse sections of whole hearts, with basement membrane indicated in white, red lines show the boundary of the compact wall of the heart, and dashed red lines highlight the orientation of cardiac muscle surrounding the left ventricle. Scale bar represents 50µm. **(B)** Representative micrographs of P5 control and SMA mouse hearts immunostained for collagen IV to show the basement membrane. High power representative images of collagen IV (red) and DAPI nuclei (blue) staining of the heart wall of the left ventricle and of trabeculations projecting into the lumen of the left ventricle. Scale bar represents 50µm. **(C)** Quantitative Western blot showing total levels of collagenIV, at birth (P1) in control and SMA hearts. Error bars, mean ±SEM (n≥3 mice per group). Unpaired student two-tailed *t*-test was used to calculate *p*-values.

Figure 3:

SMA Hearts Have a Decreased Number of Cardiomyocytes and an Increase in Apoptosis

(A) Panels show co-immunostaining of nuclei of the cardiomyocytes with DAPI (blue) and Ki67 (red) to indicate dividing cells in control and SMA hearts, at birth (P1), pre-symptomatic (P3) and early-symptomatic (P5) ages, at low (i,ii) and high power (iii,iv). Scale bar represents 50µm. **(B)** Cardiomyocyte cell density, from nuclear counts, expressed per field of view in control and SMA hearts, at birth (P1), pre-symptomatic (P3) and early-symptomatic (P5) ages. **(C)** Dividing cells (Ki67 positive nuclei) expressed as a percentage of the total number of nuclei per field of view in control and SMA hearts, at birth (P1), pre-symptomatic (P3) and early-symptomatic (P5) ages. **(D)** Quantitative Western blot showing total levels of caspase-3 in control and SMA hearts, at birth (P1), pre-symptomatic (P3) and early-symptomatic (P5) ages.

Error bars, mean ±SEM (n≥3 mice per group). Unpaired student two-tailed *t*-test and a two-way ANOVA were used to calculate *p*-values.

910
911 **Figure 4:**
912 **Oxidative Stress is Present in SMA Hearts**
913 **(A)** Quantitative Western blot showing the total levles of angiotensin II receptor 1 (AT-1) in
914 control and SMA hearts, at birth (P1), pre-symptomatic (P3) and early-symptomatic (P5)
915 ages. **(B)** Quantitative Western blot showing total levels of mitochondrial ATPsynthase FO
916 subunit 6, at birth (P1) in control and SMA hearts.
917 Error bars, mean ±SEM (n≥3 mice per group). Unpaired student two-tailed *t*-test was used to
918 calculate *p*-values.
919
920
921 **Figure 5:**
922 **Heart Microvasculature is Significantly Decreased in SMA**
923 **(A)** Representative micrographs of microvasculature seen in transverse sections of control
924 and SMA hearts, stained with GSL-1, at birth (P1), pre-symptomatic (P3), early symptomatic
925 (P5) and late-symptomatic (P8) ages. White indicates vasculature. Scale bar represents
926 50μm. **(B)**High power images of microvasculature in the left ventricular wall of P5 control
927 and SMA hearts; showing GSL-1 only (red) (i,ii) and merged with DAPI nuclei (blue) (iii,iv).
928 Scale bar represents 50μm. **(C)** Quantitative Western blot showing total PECAM-1 level in
929 control and SMA hearts, at birth (P1), pre-symptomatic (P3) and early-symptomatic (P5)
930 ages. Error bars, mean ±SEM (n≥3 mice per group). Unpaired student two-tailed *t*-test was
931 used to calculate *p*-values.
932
933 **Figure 6:**
934 **SMA Hearts are Congested with Blood Post-Mortem**
935 **(A)** Representative micrographs of transverse sections of P5 control and SMA hearts, stained
936 with Ly76 positive cells to indicate RBC and their precursors, at low (a and b) and high power
937 (c and d). Scale bar represents 50μm. **(B)** Quantification of Ly76 positive cells expressed as a
938 percentage of cross-sectional area of the heart in control and SMA, at birth (P1), pre-
939 symptomatic (P3) and early-symptomatic (P5) ages.
940 Error bars, mean ±SEM (n≥3 mice per group). A two-way ANOVA was used to calculate *p*-
941 values.
942
943 **Figure 7:**
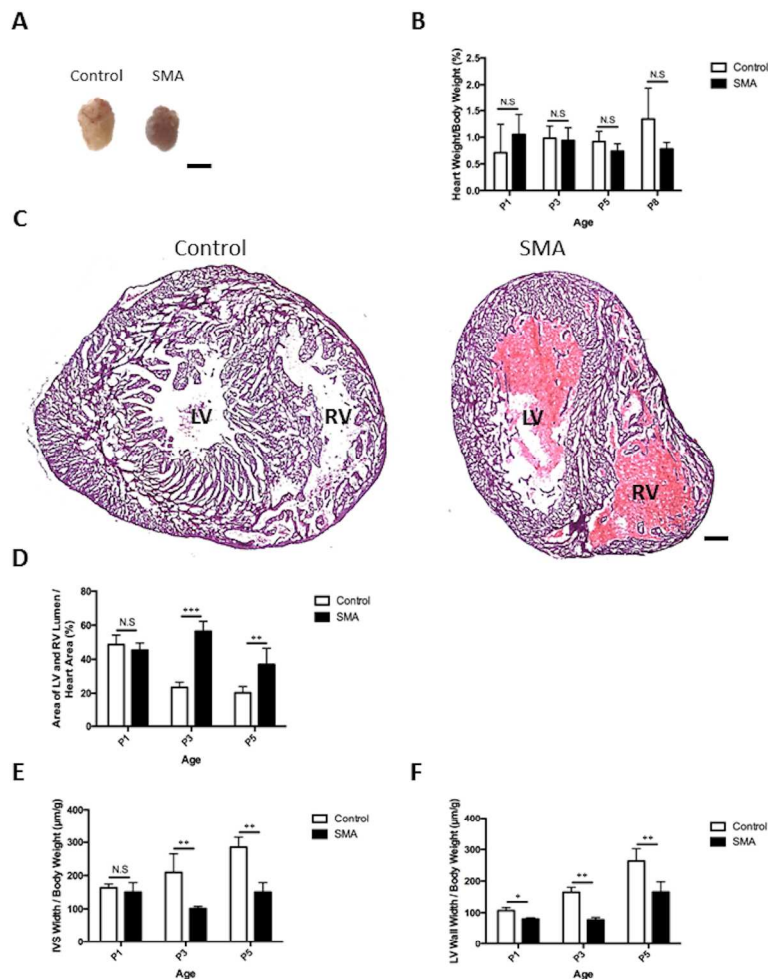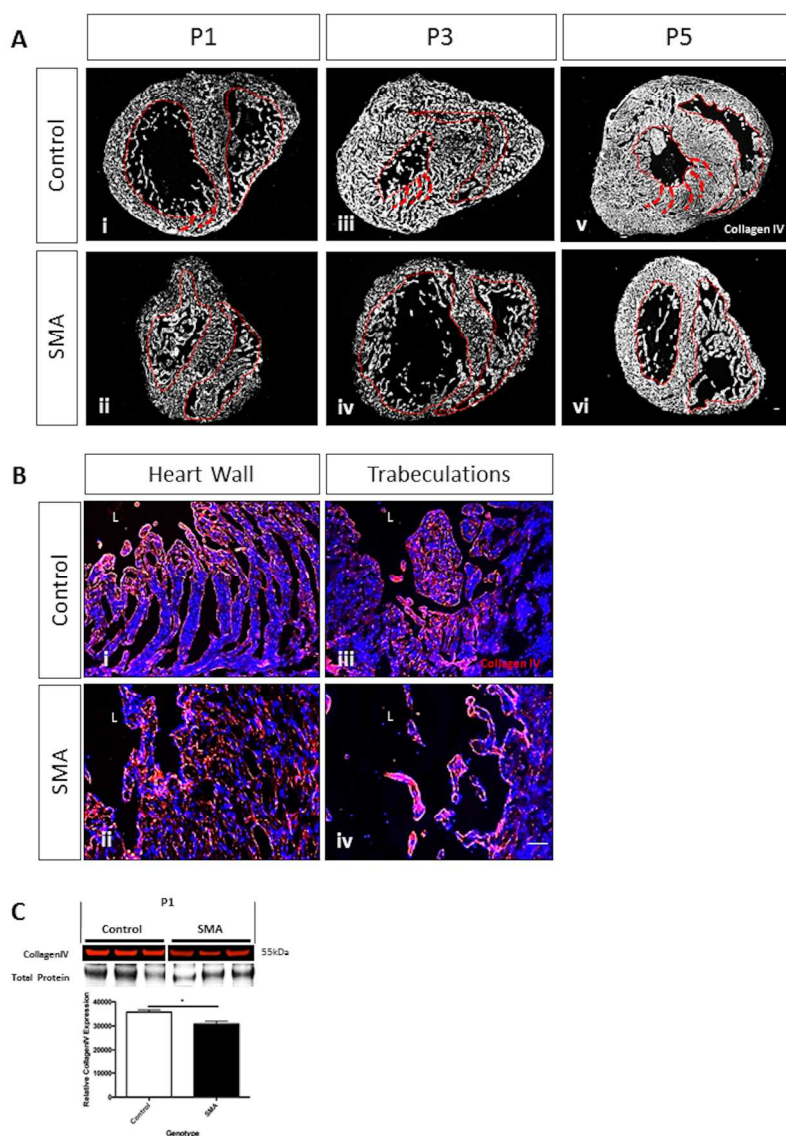944 **Proposed Model for Cardiac Defects in SMA**
945

Figure 1:
Gross Morphology of the Heart is Altered in SMA
(A) Representative images of early-symptomatic P5 hearts from heterozygous control and SMA disease mice. Scale bar represents 5mm. (B) Weight of control and SMA heart, expressed as as a % of body weight, at birth (P1), pre-symptomatic (P3), early-symptomatic (P5) and late-symptomatic ages (P8). (C) Transverse sections through the ventricles of early-symptomatic P5 hearts of control and SMA mice stained with H&E, LV= left ventricle, RV = right ventricle, scale bar represents 200μm. (D) Cross-sectional area of both ventricles, expressed as a % of total cross sectional area of heart in control and SMA mice at birth (P1), pre-symptomatic (P3) and early-symptomatic (P5) ages. (E) Width of interventricular septum (IVS) in relation to body weight of control and SMA mice at birth (P1), pre-symptomatic (P3) and early-symptomatic (P5) ages. (F) Width of LV wall in relation to body weight of control and SMA mice at birth (P1), pre-symptomatic (P3) and early-symptomatic (P5) ages.
Error bars, mean ±SEM (n≥3 mice per group). A two-way ANOVA was used to calculate p-values.
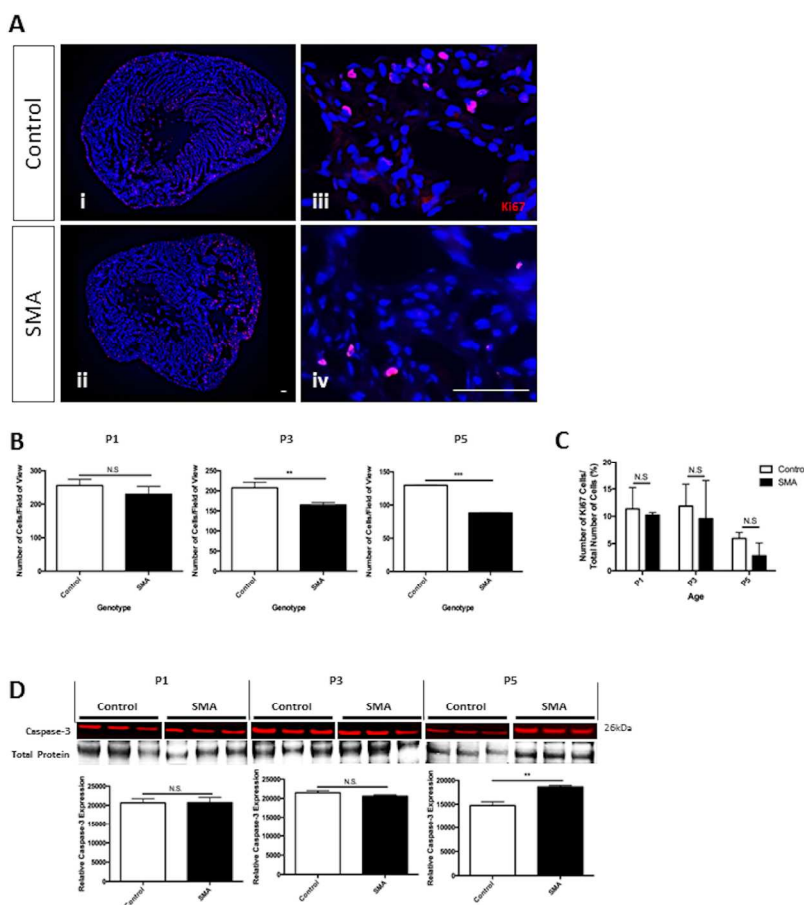
190x275mm (300 x 300 DPI)

Cardiomyocytes are Disorganised in the SMA Heart
(A) Representative micrographs in control and SMA hearts, at birth (P1), pre-symptomatic (P3) and early-symptomatic (P5) ages, immunostained for collagen IV to show the basement membrane. Images show transverse sections of whole hearts, with basement membrane indicated in white, red lines show the boundary of the compact wall of the heart, and dashed red lines highlight the orientation of cardiac muscle surrounding the left ventricle. Scale bar represents 50μm. (B) Representative micrographs of P5 control and SMA mouse hearts immunostained for collagen IV to show the basement membrane. High power representative images of collagen IV (red) and DAPI nuclei (blue) staining of the heart wall of the left ventricle and of trabeculations projecting into the lumen of the left ventricle. Scale bar represents 50μm. (C) Quantitative Western blot showing total levels of collagenIV, at birth (P1) in control and SMA hearts. Error bars, mean ±SEM (n≥3 mice per group). Unpaired student two-tailed t-test was used to calculate p-values.
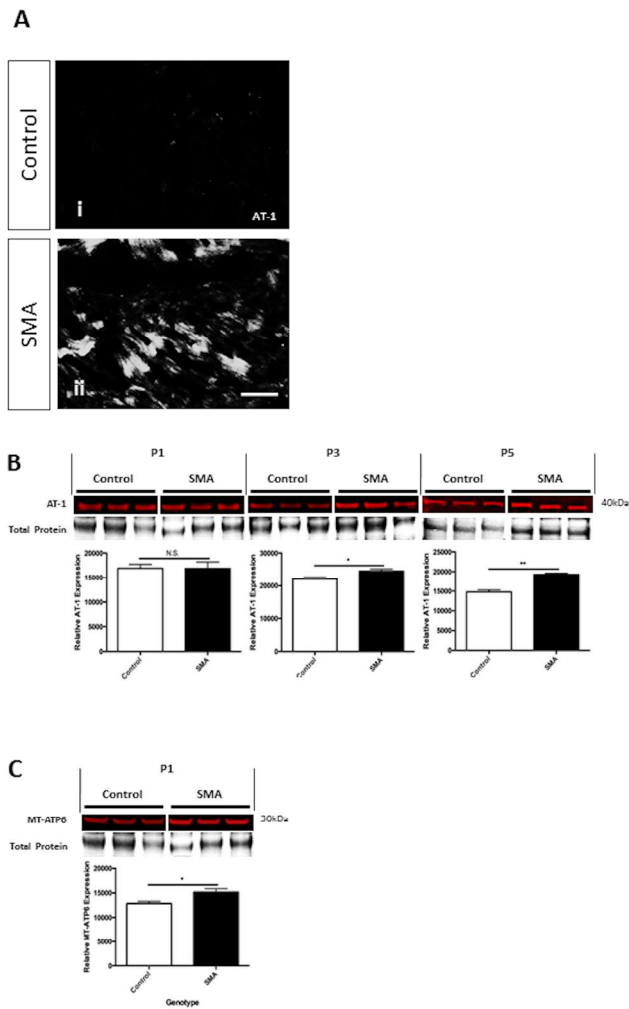
190x275mm (300 x 300 DPI)

SMA Hearts Have a Decreased Number of Cardiomyocytes and an Increase in Apoptosis
(A) Panels show co-immunostaining of nuclei of the cardiomyocytes with DAPI (blue) and Ki67 (red) to indicate dividing cells in control and SMA hearts, at birth (P1), pre-symptomatic (P3) and early-symptomatic (P5) ages, at low (i,ii) and high power (iii,iv). Scale bar represents 50μm. (B) Cardiomyocyte cell density, from nuclear counts, expressed per field of view in control and SMA hearts, at birth (P1), pre-symptomatic (P3) and early-symptomatic (P5) ages. (C) Dividing cells (Ki67 positive nuclei) expressed as a percentage of the total number of nuclei per field of view in control and SMA hearts, at birth (P1), pre-symptomatic (P3) and early-symptomatic (P5) ages. (D) Quantitative Western blot showing total levels of caspase-3 in control and SMA hearts, at birth (P1), pre-symptomatic (P3) and early-symptomatic (P5) ages.
Error bars, mean ±SEM (n≥3 mice per group). Unpaired student two-tailed t-test and a two-way ANOVA were used to calculate p-values.

190x275mm (300 x 300 DPI)

A

B

C

Oxidative Stress is Present in SMA Hearts
(A) Quantitative Western blot showing the total levles of angiotensin II receptor 1 (AT-1) in control and SMA hearts, at birth (P1), pre-symptomatic (P3) and early-symptomatic (P5) ages. (B) Quantitative Western blot showing total levels of mitochondrial ATPsynthase FO subunit 6, at birth (P1) in control and SMA hearts. Error bars, mean ±SEM (n≥3 mice per group). Unpaired student two-tailed t-test was used to calculate p-values.

190x275mm (300 x 300 DPI)
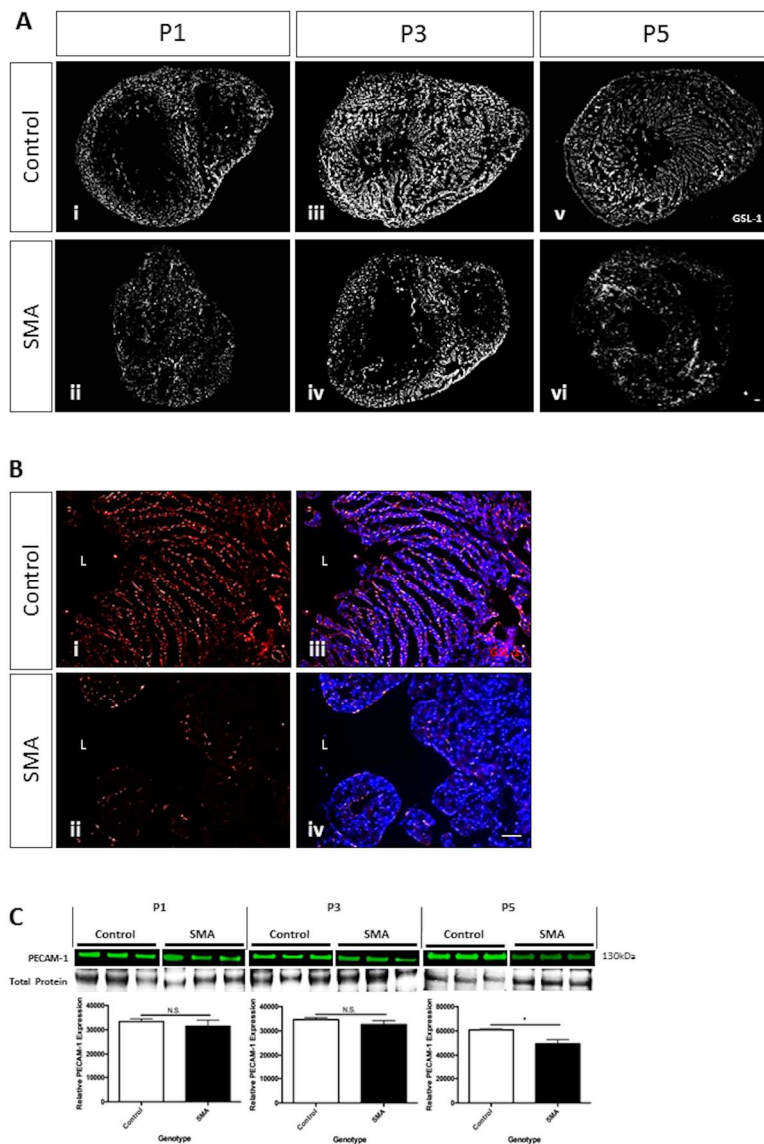
Heart Microvasculature is Significantly Decreased in SMA

(A) Representative micrographs of microvasculature seen in transverse sections of control and SMA hearts, stained with GSL-1, at birth (P1), pre-symptomatic (P3), early symptomatic (P5) and late-symptomatic (P8) ages. White indicates vasculature. Scale bar represents 50µm. (B)High power images of microvasculature in the left ventricular wall of P5 control and SMA hearts; showing GSL-1 only (red) (i,ii) and merged with DAPI nuclei (blue) (iii,iv). Scale bar represents 50µm. (C) Quantitative Western blot showing total PECAM-1 level in control and SMA hearts, at birth (P1), pre-symptomatic (P3) and early-symptomatic (P5) ages. Error bars, mean ±SEM (n≥3 mice per group). Unpaired student two-tailed t-test was used to calculate p-values.
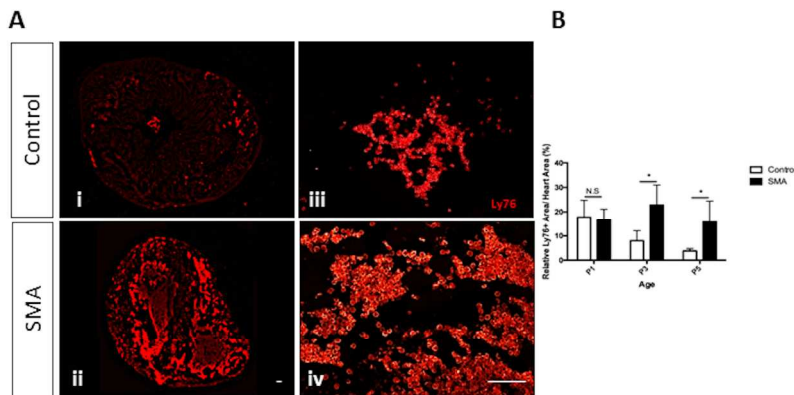
190x275mm (300 x 300 DPI)

Figure 6:
SMA Hearts are Congested with Blood Post-Mortem
(A) Representative micrographs of transverse sections of P5 control and SMA hearts, stained with Ly76 positive cells to indicate RBC and their precursors, at low (a and b) and high power (c and d). Scale bar represents 50µm. (B) Quantification of Ly76 positive cells expressed as a percentage of cross-sectional area of the heart in control and SMA, at birth (P1), pre-symptomatic (P3) and early-symptomatic (P5) ages. Error bars, mean ±SEM (n≥3 mice per group). A two-way ANOVA was used to calculate p-values.
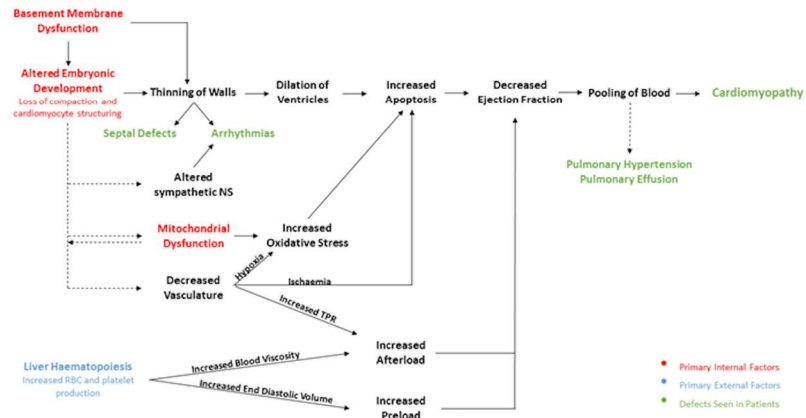
190x275mm (300 x 300 DPI)

Figure 7:
Proposed Model for Cardiac Defects in SMA

190x275mm (300 x 300 DPI)